Fredrik Fang Liland

Wake flow and aerodynamic performance of time trial helmets

Master's thesis in Mechanical Engineering

June 2019

Master's thesis

NTNU
Norwegian University of Science and Technology
Faculty of Engineering
Department of Energy and Process Engineering

NTNU
Norwegian University of
Science and Technology

Fredrik Fang Liland

Wake flow and aerodynamic performance of time trial helmets

Master's thesis in Mechanical Engineering
Supervisor: Jason Hearst, Luca Oggiano
June 2019

Norwegian University of Science and Technology
Faculty of Engineering
Department of Energy and Process Engineering

NTNU
Norwegian University of
Science and Technology

Abstract

Air resistance is the most important resistive force in bicycle racing. As an attempt to improve performance, competitive cyclists use time trial helmets that are shaped specifically to reduce air resistance. The time trial helmets that are available on the market today come in a variety of shapes, and there in no general consensus as to how the helmet should be designed to gain optimal aerodynamic performance. Studies on helmet aerodynamics have mostly been focused on measuring the difference in drag force between different helmets, but few attempts have been made in exploring the flow field around the helmet to gain insight in the mechanisms behind why different helmets perform differently.

This aim of this thesis is to investigate the flow field around the helmet when helmet geometry is changed. A survey of the wake behind the rider is carried out in order to gain insight on what effect the helmet has on the wake, and how the wake changes with different helmet geometry. In order to evaluate the effects of design parameters on aerodynamic performance, a parameter study has been carried out by use of CFD simulations. Key parameters are isolated and evaluated systematically with the aim of uncovering general relationships between design parameters and aerodynamic performance.

Wind tunnel measurements were carried out using hot wire anemometry, and the wake behind the rider using two different helmets have been characterized in terms of velocity and turbulence intensity. It was found that the helmet gives a significant contribution to the overall wake behind the rider. Comparing the wakes of a shorter and longer helmet, it has been shown that the shorter helmet generate a stronger wake than the longer helmet. The measurements also suggested that vortex shedding was generated by the short helmet.

A systematic parameter study was carried out by use of CFD simulations, where the effect of key parameters on aerodynamic performance was explored. This parameter study suggests a general trend that air resistance decreases with increasing length and width of the helmet. However, the parameter study indicates that more subtle effects are in play, as not all test cases followed this relation.

Contents

List of Figures

Chapter 1

Introduction

In cycling, there are several types of resistive forces the rider has to fight against in order to get to the finish line as fast as possible. These resistive forces include rolling resistance and drive train friction, but by a large margin, the most important force to overcome is the air resistance. At high speeds, air resistance is said to account for up to 90% of the total force the rider is subjected to [1]. The cycling industry goes to great lengths to reduce air resistance. By looking at bicycles used for competitive racing, and particularly those used in time trial races, it is clear that every component is designed with aerodynamics in mind. This is also true for other equipment and apparel the rider wears. Numerous studies have been conducted in the endeavour of reducing air resistance in cycling. As one of the first to look at aerodynamics in cycling, Nonweiler carried out wind tunnel experiments on a cyclist in a racing position [2]. Di Prampero et. al (1979) [3], Pugh (1974) [4], and Kyle and Burke (1984) [5], are other early investigators of general cycling aerodynamics.

Aerodynamics of bicycle helmets have been taken seriously the last few decades. It became a subject of great interest especially after the final time trial stage of the 1989 Tour de France. The race that year the closest race still to this day, where the winning margin between first and second place was only 8 seconds. Greg Lemond took over the lead from Laurent Fignon in the last time trial stage, and it appeared as this was achieved as a result of aerodynamic considerations. Whereas Fignon rode the stage using a standard bicycle, and his ponytail freely flapping in the wind, Lemond used both aerodynamic handlebars and an eye-catching tear-drop shaped helmet. Since then, tear-drop shaped helmets have become the norm in time trial races. However, the helmets that are available on the marked today shows a large variation in geometry. Different approaches and ideas give rise to a variety of helmet shapes. For instance, in the last few years, helmet manufacturers have started experimenting with drastically shorter helmets based on the realization that the rider may not always keep the head in the optimal position.

In addition to studies of general cycling aerodynamics, a few studies focusing specifically on time trial helmets have been carried out. Kyle and Burke (1989) found that a time trial helmet does indeed perform better than wearing no helmet [6]. Alam et. al. (2010) measured the drag coefficient of several helmets, including two time trial helmets, and found significant performance differences [7]. In a study by Chowdhury et. al. (2014), a similar investigation was carried out on five time trial helmets [8]. Again, significant differences was found. Ventilation holes and helmet length were identified as important

factors of aerodynamic performance.

Most studies on cycling aerodynamics have involved measuring the drag force of the rider. This is an obvious approach as the drag force is directly linked with the performance of the cyclist. By comparing the drag force of different helmets, it is easy to conclude which one performs better. However, measurements of drag force gives little insight into the mechanisms behind the performance difference. From such studies, it is difficult to explain why one helmet performs better than another. One approach that is thought to give better insight into the aerodynamic mechanisms behind the performance differences is to measure the flow field around the rider.

An effort to measure the full flow field around the cyclist was made by Crouch et. al. (2014), where it was explored how different leg position changes the flow structure around the rider [9]. Another study targetet helmet wakes more directly. Chabroux et. al. (2010) carried out PIV measurements of the immediate wake of the helmet to identify factors that may provide drag reduction [10].

The aim of this thesis is to investigate how a time trial helmet influence the air flow around it. A thorough survey is made of the wake behind the rider in order to gain insight on what effect the helmet has on the wake, and what differences can be seen in the wake with helmets of different shape. In order to evaluate the effects of design parameters on aerodynamic performance, a parameter study has been carried out by use of CFD simulations. Key parameters are isolated and evaluated systematically with the aim of uncovering general relationships between design parameters and aerodynamic performance.

Chapter 2

Theory

In this chapter theoretical concepts that are relevant to the present work is presented.

2.1 Air resistance

The most important resistive force in cycling is the air resistance, or aerodynamic drag. This is a force any object is subjected to when moving through air, which acts in the opposite direction of the relative motion of the object, thus slowing it down.

Air resistance is often thought of as a combination of pressure drag and skin friction drag. Pressure drag is associated with the shape of the object, and is the result of a difference in pressure on the front and back of the object. Higher pressure in front of the object than behind cause a net force acting backwards. This pressure difference is in most cases caused by flow separation, which is a phenomenon that occurs when the boundary layer is no longer sustainable under an adverse pressure gradient. When flow separates, streamlines of the flow no longer follow the surface of the object, and vortices and eddies form in the separated region. The pressure is low within this separated region, leading to the pressure difference associated with pressure drag. To avoid flow separation, to reduce pressure drag, the object should have a streamlined shape with a surface that guides the flow gently around its corners. A more gentle the curvature around the features of the object reduces the adverse pressure gradient, making flow separation less likely to occur.

Skin friction drag is the tangential force acting on the surface of the object when it is moving through a viscous fluid. The fluid sticks to the surface of the object, which cause a shear force on the surface when the object is moving. The total resistive force caused by skin friction is mostly dependent on the wetted area of the object, and for streamlined shapes skin friction drag is the biggest contributor to air resistance. For blunt objects however, such as a cyclist, pressure drag is the dominating source of resistance.

The total drag force acting on an object moving through a fluid is most commonly expressed as

$$D = \frac{1}{2}\rho v^2 C_d A \tag{2.1}$$

where ρ is the density of the fluid, v the velocity of the object relative to the fluid, A the cross-sectional area of the object, and C_d the dimensionless drag coefficient.

2.2 Boundary layers

The concept of a boundary layer relates to the region of fluid close to the surface in which effects of viscosity are important. Viscous effects become important when there is high shear in the flow, which is the case in the transitional region between stationary fluid (relative to the surface) at the surface and the outer flow.

The boundary layer thickness is most often defined as the distance from the surface where the flow has reached 99% of the free stream velocity, i.e. where $u = 0.99u_0$ [11]. For a flat plate, the boundary layer thickness for a laminar boundary layer is given as

$$\delta \approx 4.91 x \mathrm{Re}_x^{-\frac{1}{2}} . \tag{2.2}$$

If the boundary layer is turbulent, which is most likely the case in cycling aerodynamics, the boundary layer thickness is given by

$$\delta \approx 0.37 x \mathrm{Re}_x^{-\frac{1}{5}} . \tag{2.3}$$

Equation (2.3) is based on relatively crude assumptions, but gives an estimate of boundary layer thickness that is sufficient for the purpose of the present work.

2.3 CFD

The flow of fluids are governed by the Navier-Stokes equations, but due to the complexity of these equation in real life situations, it is seldom possible to get a solution for the flow analytically. With the computational technology that is available today, numerical simulations are most often used for investigating aerodynamics.

2.3.1 Governing equations

The motion of fluid is governed by the continuity equation and the Navier-Stokes equation. The continuity equation ensures that the principle of conservation of mass is fulfilled and can be written on the form

$$\frac{\partial u_i}{\partial x_i} = 0 . \tag{2.4}$$

The Navier-Stokes equation which is an expression of conservation of linear momentum, is given as [12]

$$\rho \frac{\partial u_i}{\partial t} + \rho u_j \frac{\partial u_i}{\partial x_j} = -\frac{\partial p}{\partial x_i} + \mu \frac{\partial^2 u_i}{\partial x_j \partial x_j} + \rho f_i . \tag{2.5}$$

In this application, the governing equations are simplified by the assumptions of incompressible flow and of constant viscosity. In general, conservation of energy would also be included as a governing equation, but with the assumption that temperature is constant, the energy equation is neglected.

2.3.2 Reynolds-Averaged Navier-Stokes (RANS) equation

In CFD simulations, it is in most cases impossible to fully resolve the eddies and vortices of turbulent flow. Instead, turbulence is often modelled. This can be done by use of RANS-decomposition of variables. RANS models decompose the variables of interest into a mean and fluctuating part. By introducing the decomposed definitions of velocity

$$u_i = \overline{u}_i + u_i' \tag{2.6}$$

and pressure

$$p = \overline{p} + p' \tag{2.7}$$

one can substitute these into Equation (2.5) to obtain the RANS equation [13]

$$\rho\frac{\partial \overline{u}_i}{\partial t} + \rho\frac{\partial \overline{u}_i\overline{u}_j}{\partial x_j} = \frac{\partial}{\partial x_j}\left[-\overline{p}\delta_{ij} + 2\mu\overline{S}_{ij} - \rho\overline{u_i'u_j'}\right] + \rho f_i \tag{2.8}$$

where

$$\overline{S}_{ij} = \frac{1}{2}\left(\frac{\partial \overline{u}_i}{\partial x_j} + \frac{\partial \overline{u}_j}{\partial x_i}\right). \tag{2.9}$$

A challenge with the RANS equations is the term $\overline{u_i'u_j'}$, the so-called Reynolds stress, which must be modelled. The k-ϵ turbulence model is a so-called eddy viscosity model, which is based on the concept of turbulent viscosity, and uses the Boussinesq approximation as a way to model the turbulent stresses. The Boussinesq approximation can be written on the form

$$\overline{u_i'u_j'} = \frac{2}{3}k\delta_{ij} - \nu_T\left(\frac{\partial \overline{u_i}}{\partial x_j} + \frac{\partial \overline{u_j}}{\partial x_i}\right) \tag{2.10}$$

where ν_T, the eddy viscosity, is introduced.

The k-ϵ model is a two equation model that involves solving transport equations for k and ϵ. These can be written on the form

$$\frac{\partial(\rho k)}{\partial t} + \frac{\partial(\rho k u_i)}{\partial x_i} = \frac{\partial}{\partial x_i}\left[\frac{\mu_T}{\sigma_k}\frac{\partial k}{\partial x_j}\right] + P_k - \rho\epsilon\,, \tag{2.11}$$

and

$$\frac{\partial(\rho\epsilon)}{\partial t} + \frac{\partial(\rho\epsilon u_i)}{\partial x_i} = \frac{\partial}{\partial x_i}\left[\frac{\mu_T}{\sigma_\epsilon}\frac{\partial \epsilon}{\partial x_j}\right] + C_{1\epsilon}\frac{\epsilon}{k}P_k - C_{2\epsilon}\rho\frac{\epsilon^2}{k}\,, \tag{2.12}$$

respectively, where the eddy viscosity is incorporated through the relation

$$\nu_T = C_\mu \frac{k^2}{\epsilon}\,. \tag{2.13}$$

Chapter 3

Methodology

Both wind tunnel experiments and CFD simulations have been carried out. This chapter describes the experimental setup and the methodology used in this work.

3.1 Wind tunnel

The experiments were carried out in the large wind tunnel located at the Fluid Mechanics Laboratory at NTNU. This closed-circuit wind tunnel is the largest in Norway with a cross-sectional area of 2.71×1.80m. A 220-kW centrifugal fan generate the air flow, and is capable of reaching wind speeds of up to 100km/h.

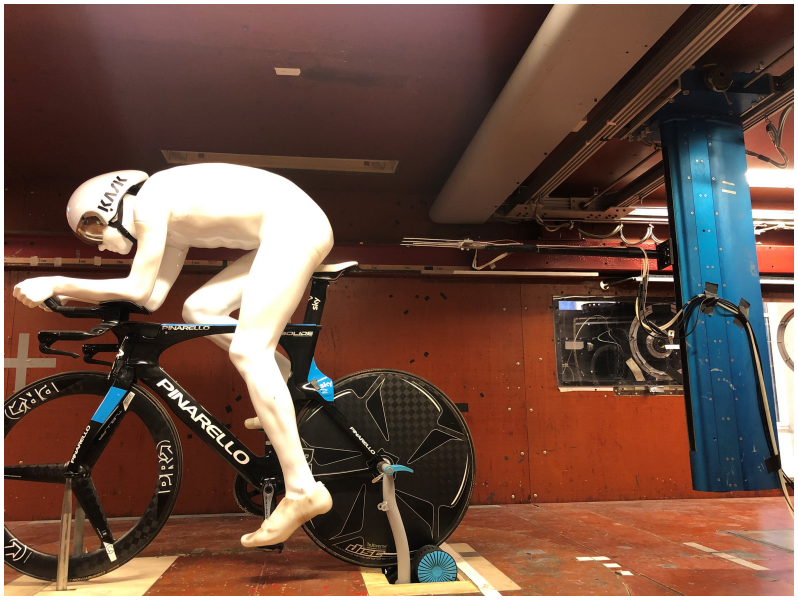

Figure 3.1: Wind tunnel experiment setup includes a full scale mannequin and hot wire probes mounted on the traverse.

Measurements of velocity and turbulence intensity in the wake of the rider in the wind tunnel were done by use of hot wire anemometry. Three single-wire hot wires were mounted to the traverse as shown in Figure (3.2).

Figure 3.2: Hot wire probes mounted on the traverse.

Even though the wind tunnel is capable of reaching high speeds, the stability of the traverse gives a limit to the possible wind speed when doing the hot wire measurements. High wind speeds cause the traverse (and thereby the hot wire probes) to vibrate, introducing inaccuracies to the measurements. A preliminary survey was carried out to find an appropriate wind speed. The chosen wind speed was chosen by the criteria that the probes did not visibly vibrate, and also that no significant peaks in the power spectrum were present. As a result, the velocity of the experiments was chosen to be 40km/h (11m/s). This velocity is close to the velocity of an actual time trial cyclist, and is assumed to represent the relevant flow regimes experienced in a cycling time trial.

The horizontal spacing of the sampling grid is slightly irregular due to limitations in available mounting positions on the traverse. Spacing between the three hot wires is 40mm and 50mm. Vertical spacing was chosen to be 50mm. Three downstream planes was chosen at locations 1D, 2D, and 3D, where L represents the torso length of the rider (640mm), which is used as a reference length scale. The resulting grid with all sample positions is shown in Figure (3.3). In addition these wake measurements, it was also carried out individual measurements with the hot wire closer to the helmet. These measurements were done with a longer sampling time to be able to look at the turbulence spectra immediately behind the helmet. They were done 10cm above the back of the rider, at 0.5D and 0D in front of the aftmost point of the rider.

Sampling time for the points in the three survey planes was 120s, whereas the two points intended for looking at turbulence spectra had a sampling time of 300s.

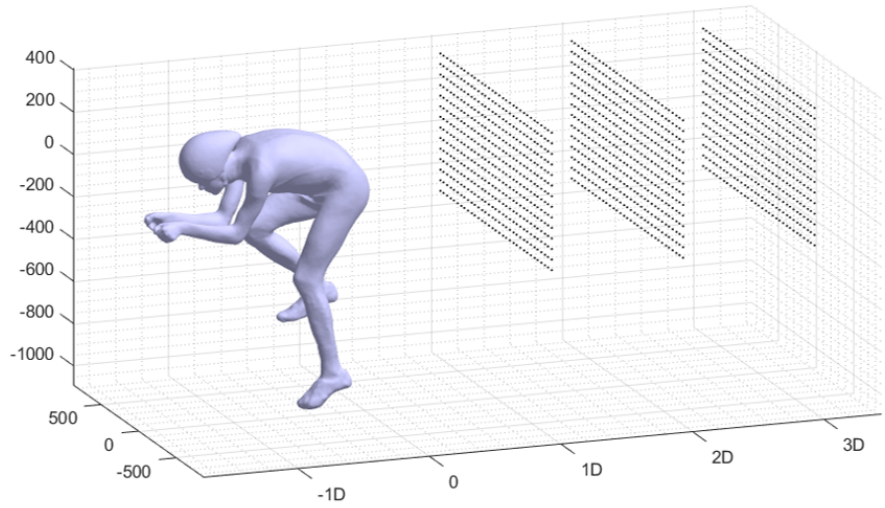

Figure 3.3: Sampling grid of wake measurements.

The subject for the wind tunnel experiments is a full scale mannequin of a cyclist in a time trial position, mounted on a time trial bicycle. No suit was put on the mannequin, so the surface of the subject is smooth.

Two helmets of different length were investigated in the wind tunnel experiment. These two helmets are provided by KASK. The helmets are publicly available under the model names Bambino and Bambino Evo, where Bambino is the shorter helmet, and Bambino Evo is the longer. These helmets will be referred to as the "Short" and "Long" helmet, respectively.

(a) KASK Bambino, Short

(b) KASK Bambino Evo, Long

Figure 3.4: The two helmets used in the wind tunnel experiments.

The measurements done in the experimental part of this thesis is not only valuable independently, but are also meant to serve as validation for CFD simulations.

3.2 CFD

3.3 Geometry model

For the parametric study of time trial helmets, a parametric geometric model was needed. The aim was to define the shape of a time trial in as simple terms as possible, while still retaining the main features of a real helmet.

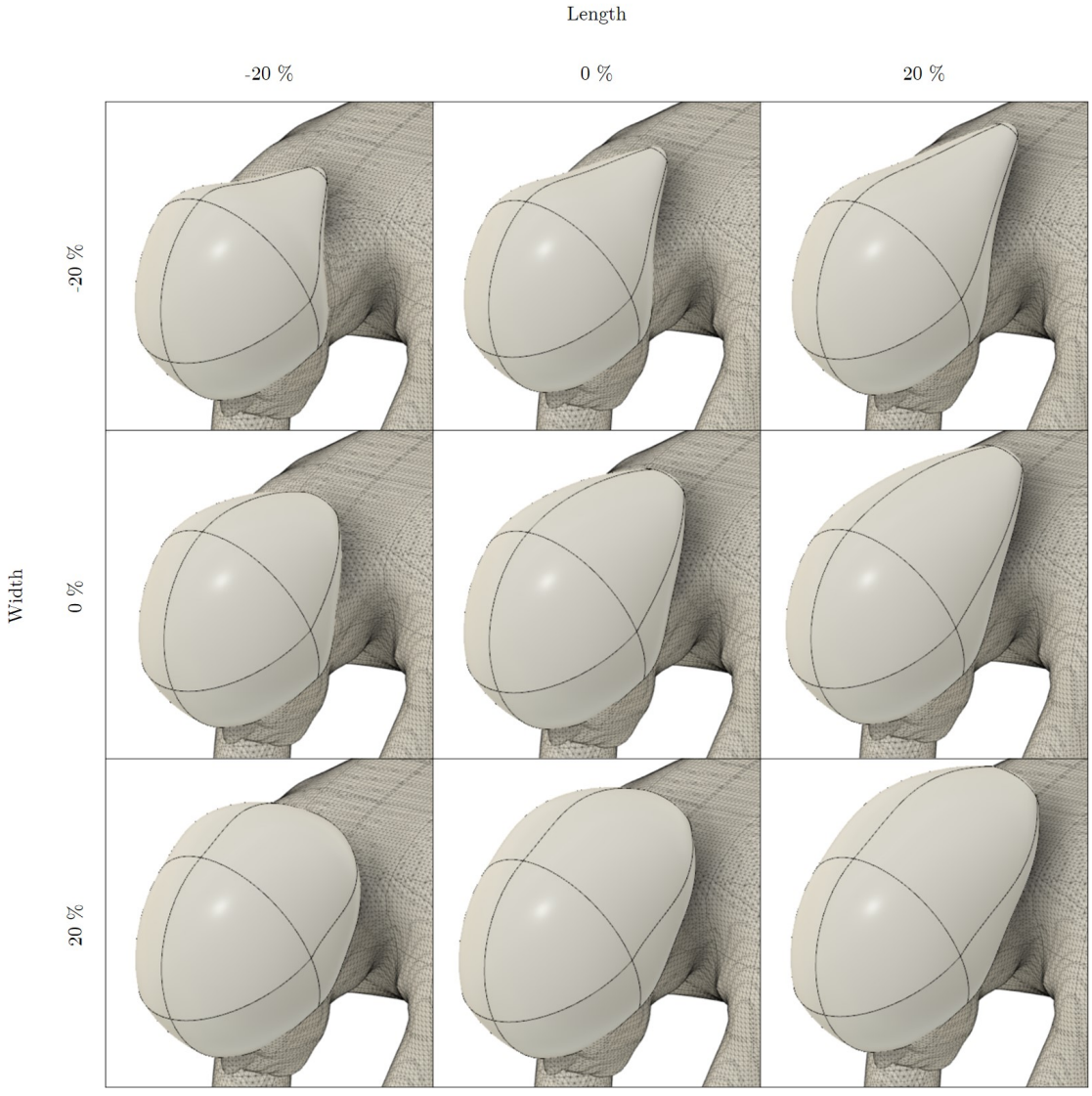

Figure 3.5: Helmet geometries of the parameter study. Generated by changing the two design parameters length and width.

Several approaches was considered when defining the geometric model. Eventually, it was decided to use a model where the helmet shape were defined in terms of a set of elliptical shapes, where altering the dimensions of the ellipses result in helmets of different geometries. To keep the parametric study simple enough, it is necessary to keep the number of parameters to a minimum. It was decided to focus on two key parameters, the

length of the tail, and the width of the tail halfway between the head and the tail end. It is believed that these parameters are ones that have the largest impact on performance.

The base case was set as the case where the dimensions closely matched the Bambino Evo, the long helmet used in the experimental part. Both length and width were altered by $\pm 10\%$ and $\pm 20\%$ to generate the test matrix. The cases that take part in the parametric study is all combinations of five different lengths and five different widths, for a total of 25 test cases. The actual geometry files were made in Fusion 360, and a selection of the resulting helmets are shown in Figure (3.5).

In addition to the simulations in the parametric study, two cases were run to serve as validation. These validation cases were run on geometries that correspond to the subjects in the wind tunnel experiment. Accurate representation of the real subject was ensured by 3D-scanning of the mannequin with each of the two helmets. It should be noted that the geometries used does not include the bicycle itself, as doing so would introduce excessive complexity to the simulations.

3.4 CFD case setup

Star-CCM+, a commersial CFD software package, was used to run the simulations. This software is widely used in industry and academics, and is especially considered to perform well with complex shapes, as the inbuilt polyhedral mesher is able to handle complex unstructured meshes well.

Due to the high computational cost of running 25 test cases (in addition to validation cases), the simulations were run on the HPC cluster Vilje. Vilje is a cluster system produced by NTNU. It has 1440 nodes, each with two 8-core Intel Sandy Bridge processors and 32GB memory.

The case setup of the simulations were to a large degree based on experience from project work, and adopts an approach similar to that of other studies [14] [15]. The simulations are steady-state, incompressible, and 3-dimensional, and for the turbulence model, the realizable k-ϵ model was used. The k-ϵ turbulence model is shown to produce good results for cycling aerodynamics. The k-ω SST model was considered and tried, but due to slower convergence than the k-ϵ model, it was not chosen. To get accurate predictions of wall friction, the two-layer wall function was used, which is capable of resolving the boundary layer provided a mesh resolution that is sufficiently fine near the walls.

Meshing was done using the Star-CCM+ polyhedral mesher. This meshing algorithm is known to perform well when dealing with complex geometries. Cell size (outside the boundary layer inflation region) was set to 4e-3m close to the surface of the rider, with gradually increasing cell size further from the subject. When the flow is expected to separate from the surface of the subject, it is necessary to have sufficiently short cells in the longitudinal direction to be able to accurately pinpoint the location at which separation occurs. When larger cell sized was attempted, this is believed to be part of the reason why issues regarding oscillating residuals arose.

The inflation layer was defined by setting an appropriate first layer height, total height, and number of inflation layers. The total height of the inflation region was set with the aim of containing the entire boundary layer of the flow. Based on an estimate from Equation (2.3), this was set to 0.01m. First layer height was set using an iterative approach

during preliminary runs, where y+ values were monitored and adjusted between each run. The aim was to achieve y+ values close to 1, to be able to resolve the boundary layer accurately. This was achieved with a first layer height set to 4e-5m. With 17 inflation layers, this first layer height and total height result in a growth rate within the inflation layer of 1.287. Figure (3.6) shows the distribution on y+ values on the surface of the rider for a typical case.

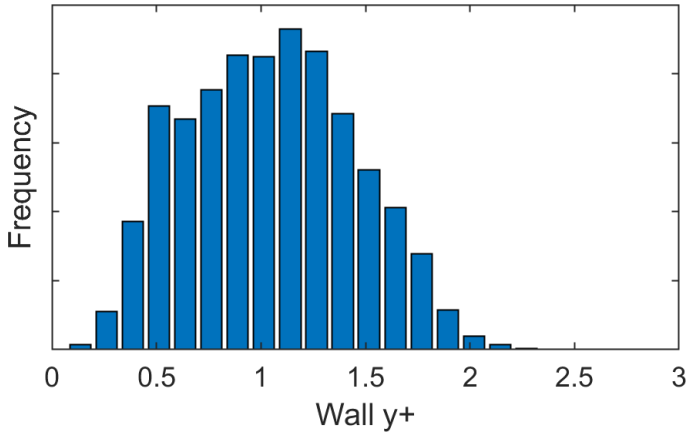

Figure 3.6: Distribution of y+ values on the surface of the subject.

The domain size was set to 10×10×20m, which with symmetry boundary conditions for the surrounding walls should be large enough that the flow around the subject does not interact with the boundaries. A velocity inlet and pressure outlet was used, with inlet conditions of 11m/s and a turbulence intensity of 0.01. It should be noted that the turbulence inlet condition is slightly lower that what is actually the case in the wind tunnel. The above mesh settings results in a total cell count of up to 20 million cells, which is at the upper level of what is viable with 32GB of per-node-memory. Even though most of the meshing algorithm is done in parallel, certain steps are done in serial, so the per-node-memory is the limiting factor rather than the total amount of memory among all nodes.

Convergence criteria was set to 1e-4 for all residuals, which was reached after 1000-2000 iterations. In addition to monitoring residual convergence, the drag force was monitored to ensure that it converged to a steady value toward the last iterations. Figure (3.7) shows the residual convergence for a typical case, and Figure (3.8) shows the drag force monitor for the same case.

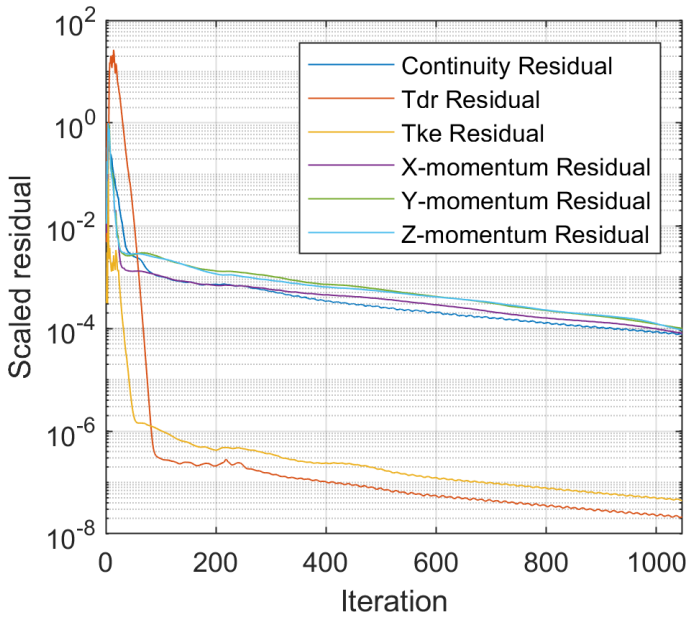

Figure 3.7: Residual convergence of CFD simulation.

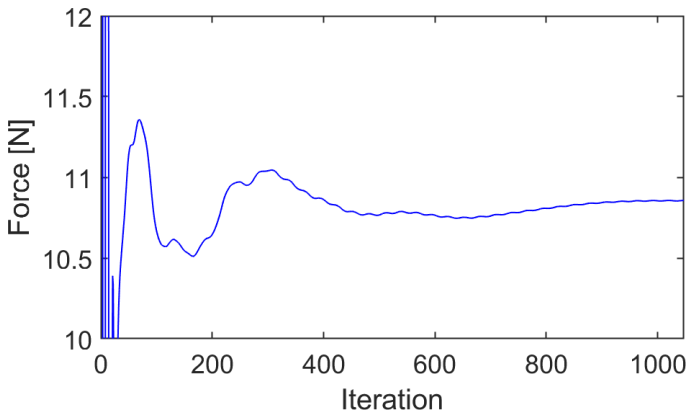

Figure 3.8: Drag force monitor.

To ensure that the CFD simulations provide credible results, the results from two validation cases was compared with measurements from the wind tunnel.

Chapter 4

Results

In this chapter, results from both wind tunnel experiments and CFD-simulations will be presented and discussed.

4.1 Wake

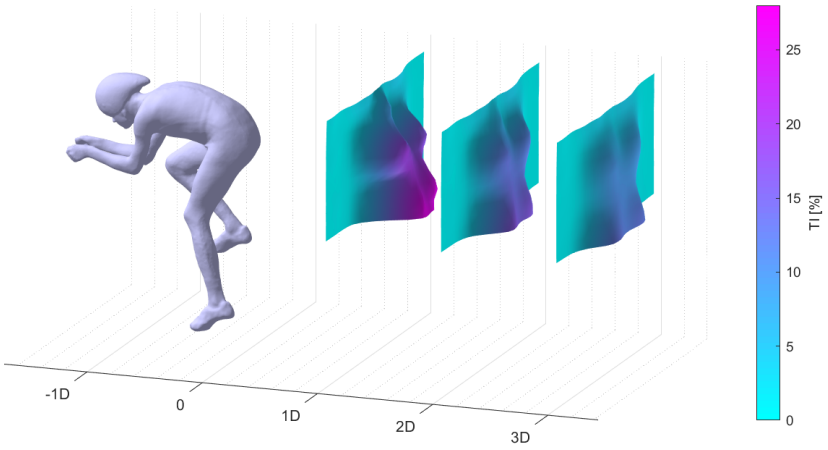

Figure 4.1: Overview of wind tunnel wake measurements.

The wake behind the rider mannequin was measured using hot wire anemometry as described in Chapter 3. Measurements of velocity and turbulence was done at three planes located at 1D, 2D, and 3D downstream of the subject for each of the two helmets. Figure (4.1) is a depiction of the spacial extent of the measurements. Contours of velocity at the three planes in the wake of the rider are shown in Figure (4.2). Similarly, contours of turbulence intensity are shown in Figure (4.3).

Clearly, the major part of the wake is generated from the body of the rider itself. It is natural that the areas of the wake associated with the shoulders and hips are most prominent, as those features of the body are large and mostly blunt. However, looking at

the upper area of the wake, it is apparent that the head does give a significant contribution to the total wake.

The velocity deficit in the area of the wake associated with the head is as high as 18% at the plane closest to the rider. For comparison, the maximum velocity deficit in the wake at this downstream location is 45%. The same point can be made by looking at the turbulence intensity. Behind the head, turbulence intensity is as high as 11%, compared to a maximum turbulence intensity in the wake of 27%. Turbulence values in the plane located at 1D, closest to the rider, should be read with a degree of scepticism as it is believed that a recirculation zone is likely to be present. However, the ratio between head turbulence and maximum turbulence still show the same effect at the planes further downstream.

Regarding the difference between the two helmets. It can be seen that the short helmet generate a stronger wake that the long helmet. The short helmet has a larger velocity deficit and a higher turbulence intensity, and the wake produced by the short helmet is also spread over a larger area. The differences in the wakes of the two helmets will be made more clear in the following.

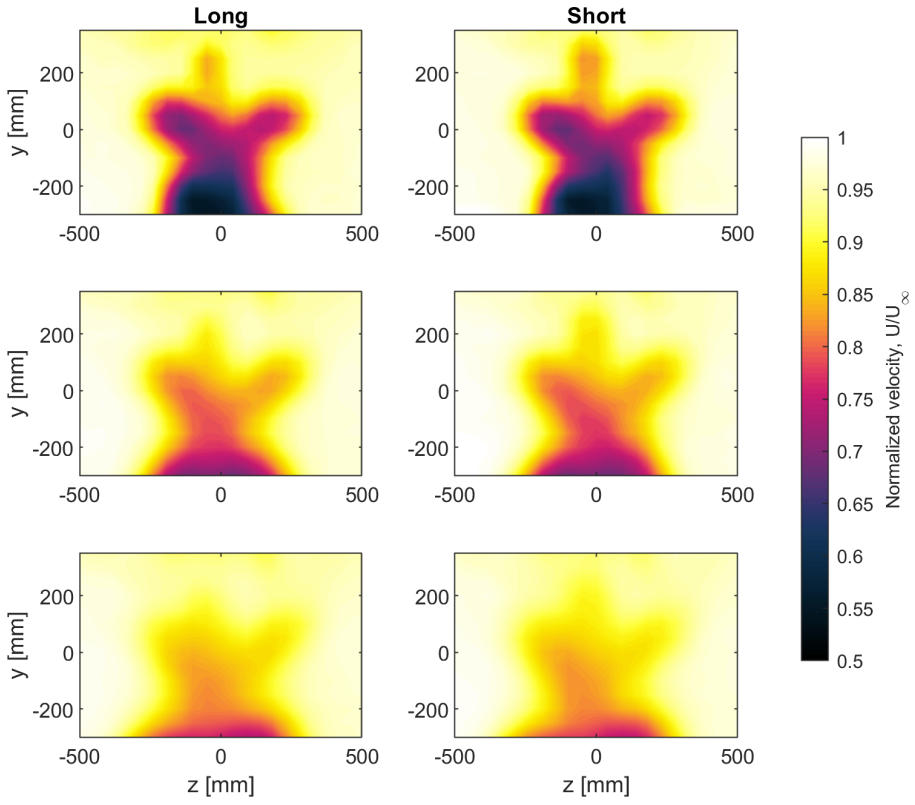

Figure 4.2: Velocity field in the wake of the rider. Long and short helmet, at 1D, 2D, and 3D.

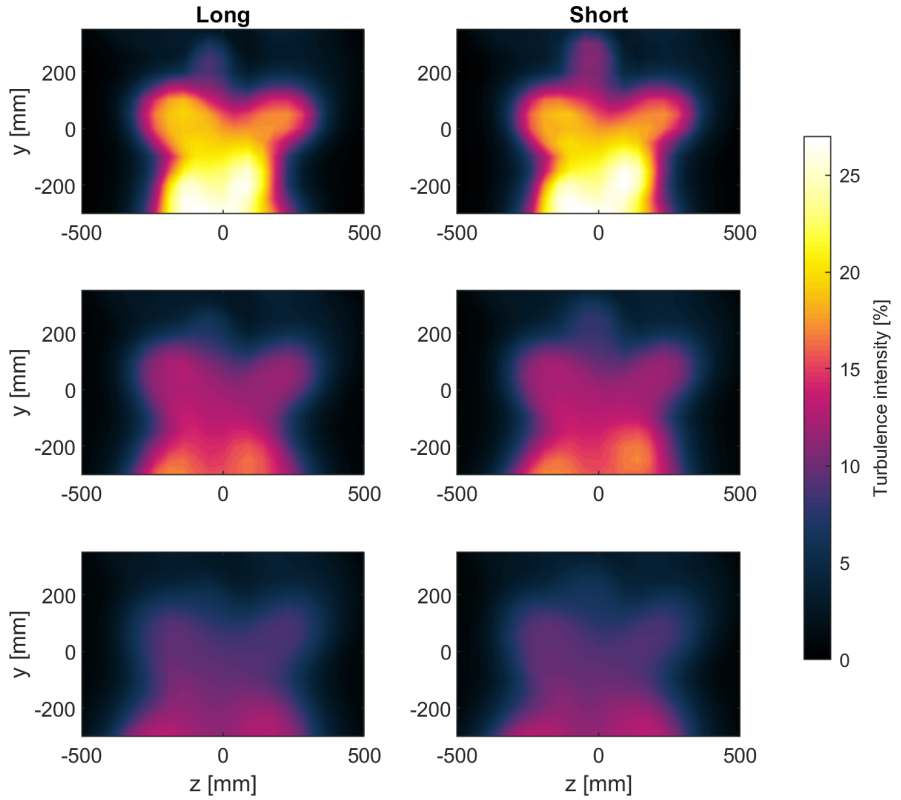

Figure 4.3: Turbulence field in the wake of the rider. Long and short helmet, at 1D, 2D, and 3D.

Looking at the velocity and turbulence profiles in the upper wake, at a height corresponding to the height of the helmet, the difference between the long and the short helmet is more clear. The short helmet generates a stronger wake than the long helmet. As Figure (4.4) show, the short helmet gives a larger velocity deficit and higher turbulence than the long helmet, suggesting that the short helmet acts as a more severe obstruction of the flow.

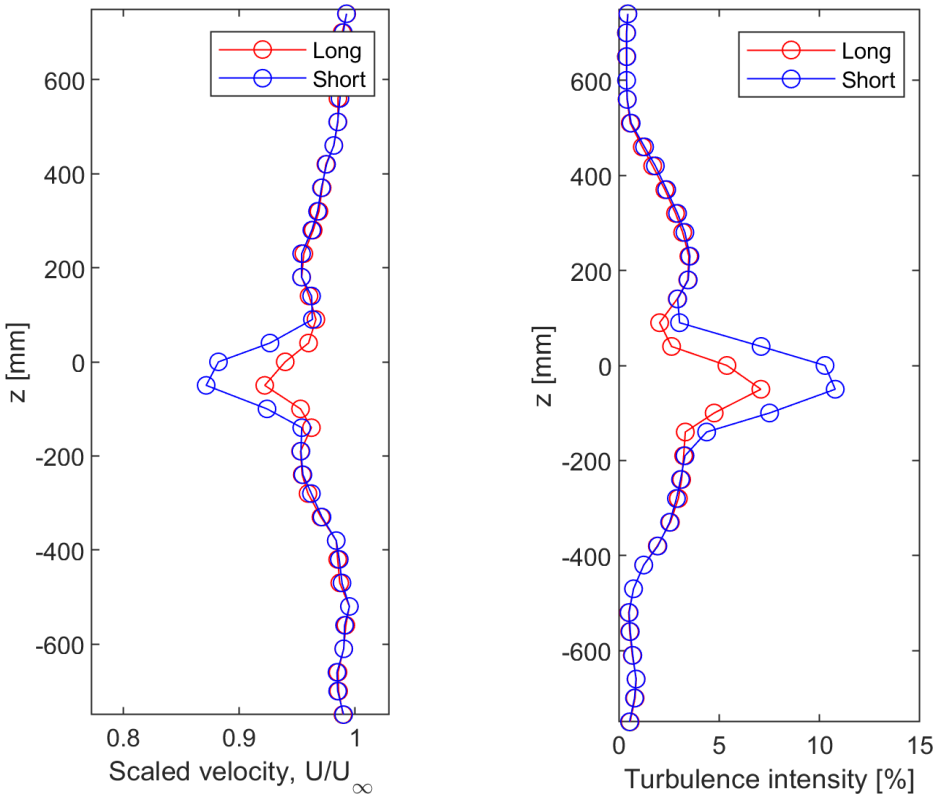

Figure 4.4: Horizontal velocity and turbulence profiles behind the short and long helmet. Measured at 1D.

Figure (4.11) shows the differences in the wake of the rider between the two helmets. In this figure, the velocity/turbulence intensity in the wake of the short helmet is subtracted from that of the long helmet. The difference is scaled with the free stream velocity and the maximum turbulence intensity (maximum among any of the three planes so that each contour plot is scaled with the same value).

Differences in the wakes mainly shows up in two locations, behind the head in the wake associated with the head, and lower in the wake at a location roughly corresponding to that of the hips of the rider. Behind the head, it is once again clear that the short helmet produce a stronger wake than the long helmet. The long helmet has 4.6% higher velocity and 18% less turbulence behind the head than the short helmet in the plane closest to the rider.

While it seems natural that there is a difference in the wake behind the helmet, differences between the two helmets show up also at a location in the lower part of the wake, which is perhaps less intuitive. The difference in the lower location is comparable in magnitude to the upper difference, and in the case of the 1D-plane, even larger.

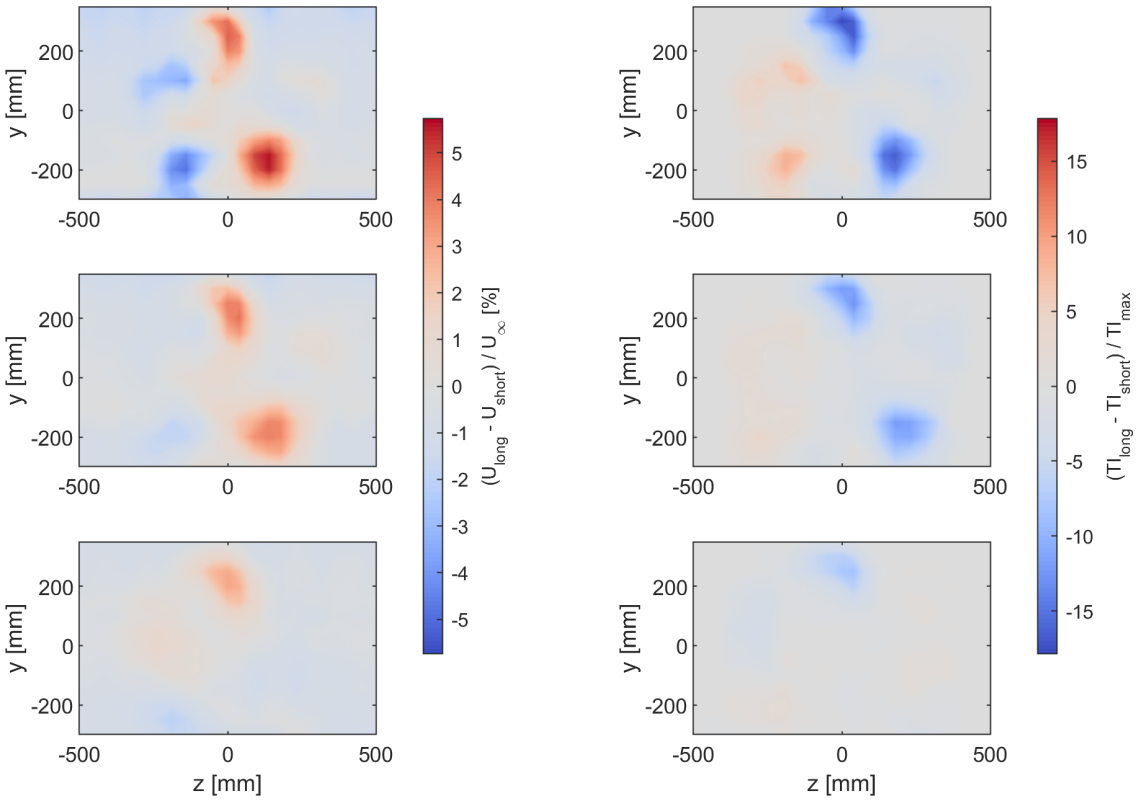

Figure 4.5: Difference in the wakes of the long and short helmet.

A feature of the lower difference is that deviations opposite in magnitude is present roughly symmetrically on either side of the wake. This suggest that the differences in the lower wake is not a result of different strength of the wake, but rather a lateral shift of the wake. Namely, the wake of the short helmet is shifted to the right (in the figure, left from the perspective of the rider) compared to the long helmet. Another feature is that the upper difference is more persistent that the lower difference. At the plane furthest downstream, the lower difference has almost vanished entirely, while the upper difference is still visible. The fact that the lower difference is a shift of the wake and the upper difference is an actual difference in strength can be thought to explain why the upper difference is more prevalent. Further, the persistence of the upper difference indicate that the difference in the upper wake is more likely to account for a difference in drag.

Even though the difference in the lower part of the wake seems counterintuitive, the presence of such a difference is supported by findings in another study. Crouch et. al. conducted wake measurements of a rider at different leg positions, and states that "the effect of leg position on the structure of the wake is not constrained to regions near the legs where movement occurs, but the entirety of the upper wake is affected" [9]. If the geometry of the lower part of the rider can affect the upper part of the wake, it seems reasonable that the geometry of the helmet can affect the lower part of the wake.

4.2 Turbulence spectra

To further explore differences in the wake of the two helmets, turbulence spectra were measured immediately downstream of each helmet as described in Chapter 3. The power spectral density of the velocity time series are shown in Figure (4.6). Notable differences can be seen in the lower frequency end of the spectrum, where the short helmet produce a higher level of turbulence. In addition, the spectrum of the short helmet has a peak at about 16Hz, which is not present for the long helmet. This peak is indicative of vortex shedding behind the short helmet.

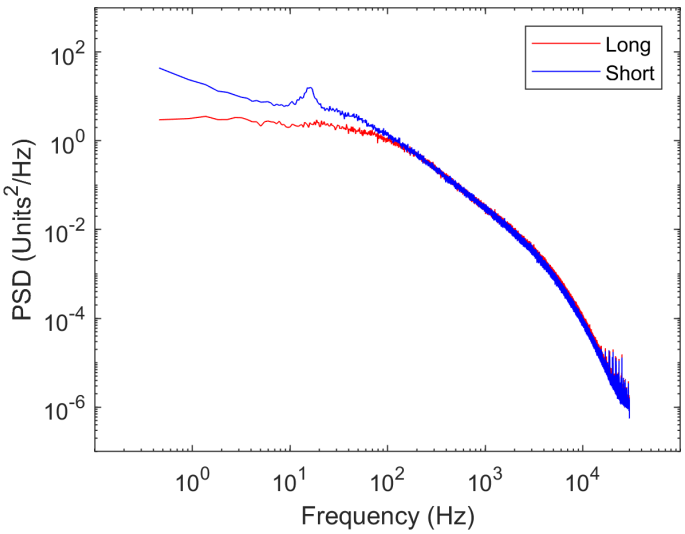

Figure 4.6: Turbulence spectra 0.5L downstream of helmets.

4.3 CFD

CFD simulations was run on two validation cases to be able to assess how well the simulations correspond with wind tunnel measurements. The subjects of these validation cases are 3D-scanned models of the mannequin with each of the two helmets. It should be noted that the simulations does not include the bicycle to reduce complexity of the simulations. Values of velocity and turbulence were extracted from three planes corresponding to those measured in the wind tunnel. Figure (4.7) shows contours of velocity at the three planes for both helmets. Similarly, Figure (4.8) shows contours of turbulence at those same locations.

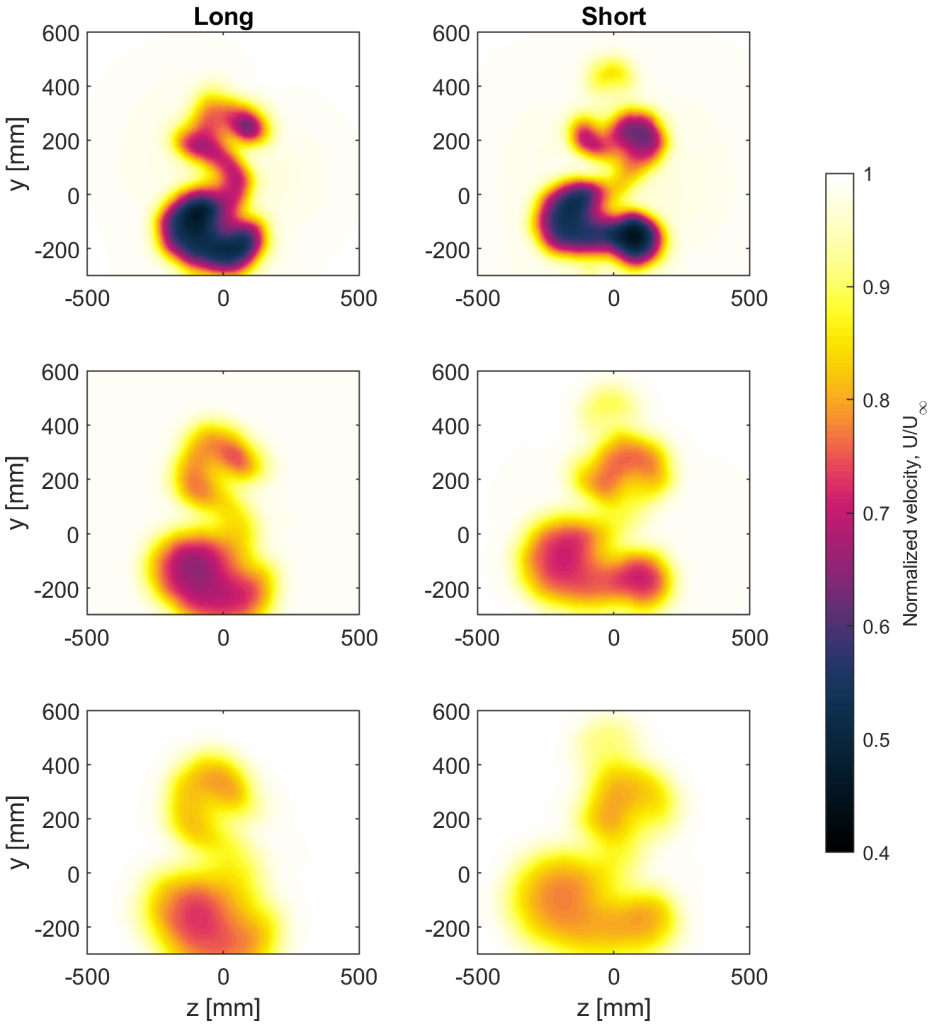

Figure 4.7: Velocity field in the wake of the rider. Long and short helmet, at 1D, 2D, and 3D.

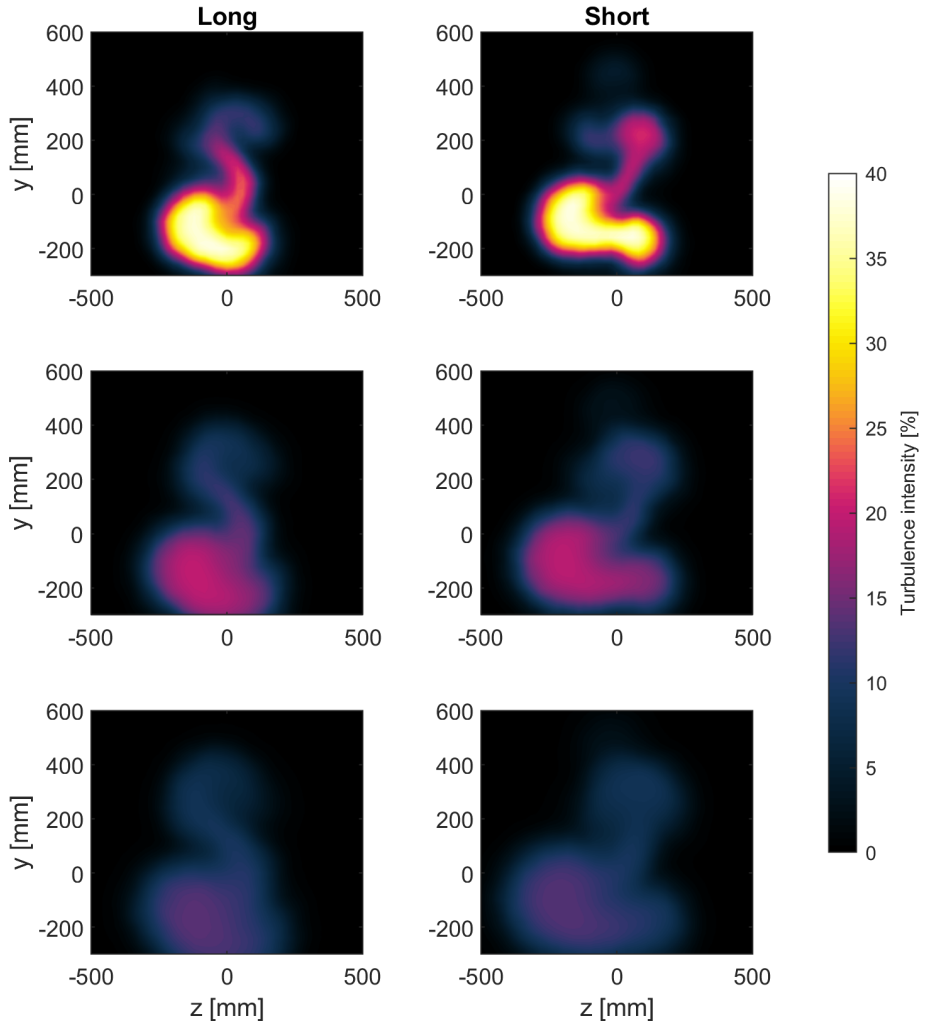

Figure 4.8: Turbulence field in the wake of the rider. Long and short helmet, at 1D, 2D, and 3D.

A comparison of the wakes from the wind tunnel measurements and the CFD simulations is shown in Figure (4.9) and (4.10). Figure (4.9) shows a comparison of velocity contours for both helmets (long above and short below) at 2D behind the rider, while Figure (4.10) shows contours of turbulence intensity correspondingly. Differences between experiments and simulations are clear. For once, the simulations give a wake that is significantly higher than that of the wind tunnel experiment. Further, the individual structures that make up the full wake are more distinct than in the wind tunnel. If one think of the wake of the rider as a cascade of wake structures from different features of the rider, it seems like these individual structures are more blended together in the wind tunnel.

The fact that the simulation wake shows up higher than that of the experiment might be a result of the roof in the wind tunnel (or rather, lack of a roof in the simulations). In fact, the highest point of the simulation wake is at a location that would correspond to a location outside the actual wind tunnel. Confinement by the roof in the wind tunnel could cause the wake to deflect downwards compared to the situation of the simulations. Another reason why the simulation wake is higher might be that the simulations does not include a bicycle. An obstruction of the flow in the lower part of the model could give

the wake a downward deflection.

There are features of the wake that are similar for in the simulations and wind tunnel experiments however. The lateral extent of the simulation wake seems to correspond well with experiments. Also, the maximum velocity deficit and turbulence intensity in each of the three planes are of a similar magnitude (apart from turbulence intensity in the closest plane, where recirculation is believed to be present).

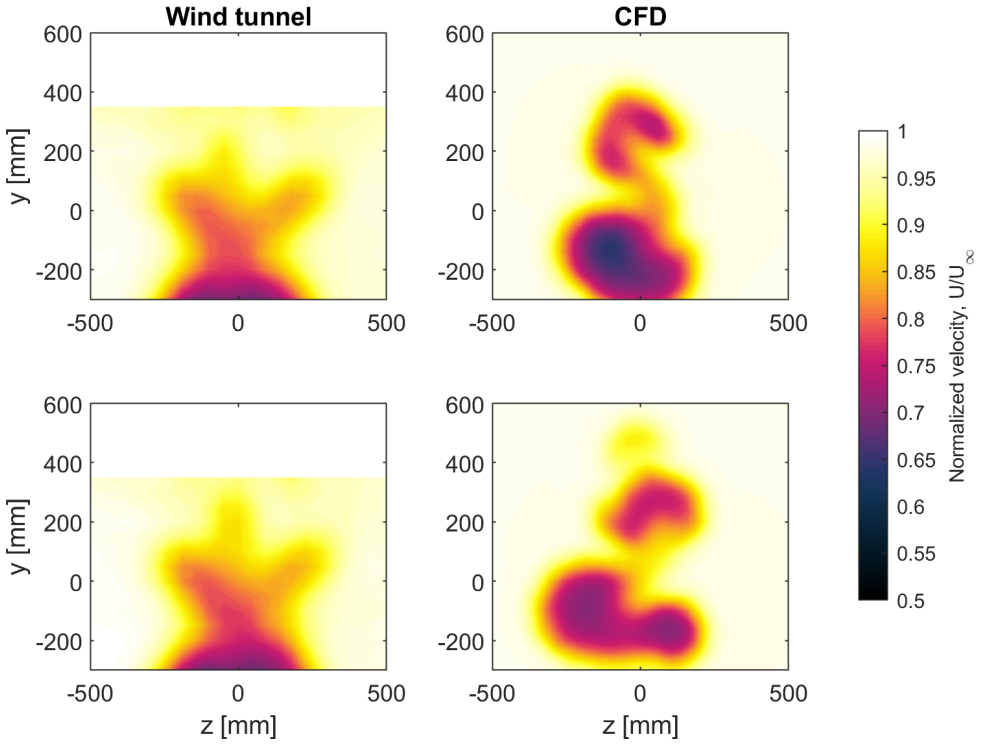

Figure 4.9: Comparison of results from wind tunnel measurements and CFD simulations. Velocity contours.

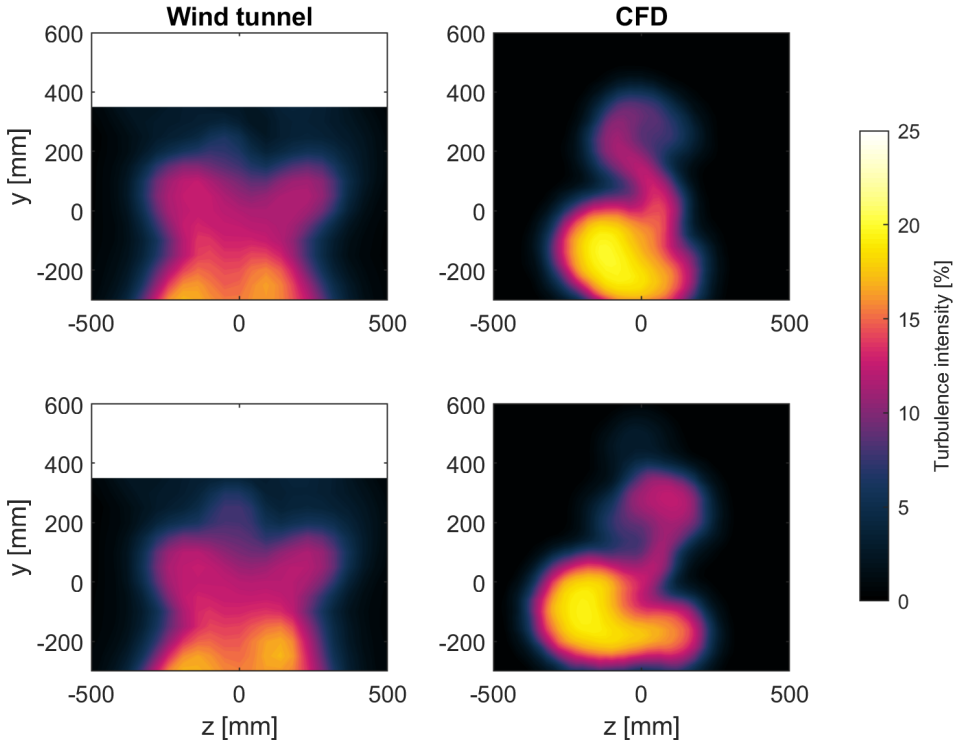

Figure 4.10: Comparison of results from wind tunnel measurements and CFD simulations. Turbulence intensity contours.

As for the wind tunnel experiment, contour plots highlighting the difference in the wakes between each helmet have been produced from the simulation results. In the simulations, as in the wind tunnel, the short helmet gives a higher velocity difference and higher turbulence in the part of the wake that is associated with the head than the long helmet. Furthermore, large differences shows up in the lower part of the wake, again indicating that the helmet geometry influence the whole wake of the rider, not only the upper part. The magnitude of the differences are much higher in the simulations than in the wind tunnel. This might be a result of the individual wake structures being less mixed than in the wind tunnel, due to lower turbulence intensity. The strength of these individual structures is of comparable magnitude, but are deflected to a slightly different location with each of the two helmets, which shows up as large differences in the figure.

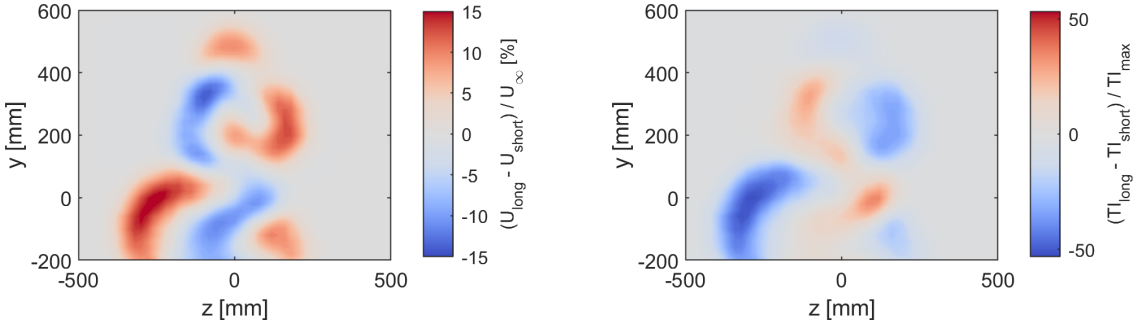

Figure 4.11: Difference in the wakes of the long and short helmet.

4.4 Parameter study

As can be seen in the previous section, results from the CFD simulations does not match the wind tunnel case exactly. This does not necessarily mean that there are plain errors in the simulations, but the following must be read with a healthy portion of scepticism (as is often the case with CFD simulations). However, even if the flow field in the wake deviate from the wind tunnel case, it can be thought that values of drag force, and in particular the difference in drag between different geometries, emulate similar effects to those that would be experienced in the real case. The difference in drag between the different helmet geometries is what this section will focus on.

The parametric study will look at the effects of two parameters, length and width, as described in Chapter 3. Using the dimensions of the long helmet, Bambino Evo, as a base case, length and width were altered with ± 10% and 20%, i.e. the test matrix include five different lengths and widths, for a total of 25 test cases. Each case were simulated according to Chapter 3, and these results are shown in Figure (4.12).

Width \ Length	-20 %	-10 %	0 %	10 %	20 %
-20 %	0,63 %	-0,36 %	0,41 %	0,08 %	-0,68 %
-10 %	-0,11 %	1,06 %	0,12 %	0,01 %	-1,17 %
0 %	1,55 %	1,44 %	0,00 %	-0,78 %	0,14 %
10 %	0,01 %	-0,03 %	-2,19 %	0,60 %	-1,81 %
20 %	1,25 %	-2,14 %	-1,06 %	-1,46 %	-1,31 %

Figure 4.12: Results of parameter study. All 25 test cases.

The values presented are percent deviation of drag force from the base case. A general trend seen from Figure (4.12) is that performance seems to increase as you move towards the bottom right corner, meaning that you are more likely to get better performance by increasing length and width than reducing those parameters. In general, increasing length and width of the helmet will result in a more gentle curvature towards the tail end of the helmet, which will likely cause the flow to stay attached further along the helmet.

Several cases does not follow the general trend of increasing performance by increasing the two parameters. For instance, an increase in length and width by 10% leads to a performance loss of 0.60%, while a reduction in length by 10% and reduction in width of 20% leads to a performance gain of 0.36%. Further, the best performing case is L=0,

W=+10, while the worst performing case is L=-20, W=0, neither of which is located in the corners of the test matrix. These examples first and foremost show that there are more subtle effects in play when it comes to the performance of these helmets, that is difficult to explain purely from the results of such a crude parameter study. The flow around the helmet is complicated, in that flow around the hands, shoulders, back, and other parts of the body interact with the flow around the helmet.

With a bit of imagination, it may seem like there exist somewhat constant diagonals in the figure. One reason why that this may be true is that the diagonals somewhat represents constant curvatures, i.e. increasing length or increasing width will have a similar effect to the curvature of the helmet in the area where separation is likely to occur.

Chapter 5

Conclusion

This thesis has investigated how different time trial helmet shapes influence the wake behind the rider. Wind tunnel experiments were carried out measuring velocities and turbulence in the wake of the rider when using different helmets. In addition, a parameter study of helmet design have been carried out to evaluate what effect changes of key design parameters have on aerodynamic performance. A parametric geometry model of a generic time trial helmet was defined. To explore the performance of the different parameter choices, CFD simulations were carried out. The measurements done as a part of this thesis are also useful for validation of CFD. A large amount of information on the flow field was collected, and the CFD simulations carried out were compared to these measurements.

Wake measurements show that the helmet generate a significant contribution to the total wake of the rider. Furthermore, it has been shown that different helmet shapes influence the wake differently. Specifically, a shorter helmet generate a stronger wake than a longer helmet, as the wake behind the shorter helmet had both higher velocity deficit and higher turbulence.

It has been shown that changing helmet geometry does not only influence the wake in the vicinity of the head. Significant differences were found in the wakes as far down as hip level.

By measuring turbulence spectra close behind the helmets, the difference in turbulence conditions behind the two helmets was shown. These measurements indicate that the shorter helmet generate vortex shedding, whereas the longer helmet does not.

Validation of CFD simulations was done by comparing the results against wind tunnel experiments. Significant discrepancies was found. Most notably, the wakes from the simulations were higher than those measured in the wind tunnel, the individual structures in the wake was more distinct in the simulations than in the measurements, and the simulations gave a bigger difference in the wakes when helmet geometry was changed.

A parameter study, focusing on length and width of the helmet was carried out. Values of drag force was presented for each of the 25 cases of the test matrix. The parameter study suggests a general trend that performance is more likely to improve by increasing the length and the width of the helmet. However, not all test cases fell within this trend, indicating that more subtle effects of the shape of the helmet have a significant effect on aerodynamic performance.

Bibliography

[1] F. Grappe, R. Candau, A. Belli, and J. D. Rouillon, "Aerodynamic drag in field cycling with special reference to the obree's position," *Ergonomics*, vol. 40, no. 12, pp. 1299–1311, 1997.

[2] T. Nonweiler, "The air resistance of racing cyclists," tech. rep., College of Aeronautics Cranfield, 1956.

[3] P. Di Prampero, G. Cortili, P. Mognoni, and F. Saibene, "Equation of motion of a cyclist," *Journal of Applied Physiology*, vol. 47, no. 1, pp. 201–206, 1979.

[4] L. G. C. E. Pugh, "The relation of oxygen intake and speed in competition cycling and comparative observations on the bicycle ergometer," *The Journal of physiology*, vol. 241, no. 3, pp. 795–808, 1974.

[5] C. R. Kyle and E. Burke, "Improving the racing bicycle," *Mechanical engineering*, vol. 106, no. 9, pp. 34–45, 1984.

[6] C. Kyle, "The aerodynamics of handlebars and helmets," *Cycling Science*, vol. 1, no. 1, pp. 22–25, 1989.

[7] F. Alam, H. Chowdhury, Z. Elmir, A. Sayogo, J. Love, and A. Subic, "An experimental study of thermal comfort and aerodynamic efficiency of recreational and racing bicycle helmets," *Procedia Engineering*, vol. 2, no. 2, pp. 2413–2418, 2010.

[8] H. Chowdhury and F. Alam, "An experimental study on aerodynamic performance of time trial bicycle helmets," *Sports Engineering*, vol. 17, no. 3, pp. 165–170, 2014.

[9] T. N. Crouch, D. Burton, N. A. T. Brown, M. C. Thompson, and J. Sheridan, "Flow topology in the wake of a cyclist and its effect on aerodynamic drag," *Journal of Fluid Mechanics*, vol. 748, pp. 5–35, 2014.

[10] V. Chabroux, M. N. Mba, P. Sainton, and D. Favier, "Wake characteristics of time trial helmets using piv-3c technique," in *15th Int. Symp. on Applications of Laser Techniques to Fluid Mechanics, Lisbon, Portugal*, vol. 58, 2010.

[11] H. Schlichting and K. Gersten, *Boundary-layer theory*. Springer, 2016.

[12] F. M. White and I. Corfield, *Viscous fluid flow*, vol. 3. McGraw-Hill New York, 2006.

[13] H. Tennekes, J. L. Lumley, J. Lumley, *et al.*, *A first course in turbulence*. MIT press, 1972.

[14] F. Beaumont, R. Taiar, G. Polidori, H. Trenchard, and F. Grappe, "Aerodynamic study of time-trial helmets in cycling racing using cfd analysis," *Journal of biomechanics*, vol. 67, pp. 1–8, 2018.

[15] T. Defraeye, B. Blocken, E. Koninckx, P. Hespel, and J. Carmeliet, "Aerodynamic study of different cyclist positions: Cfd analysis and full-scale wind-tunnel tests," *Journal of biomechanics*, vol. 43, no. 7, pp. 1262–1268, 2010.

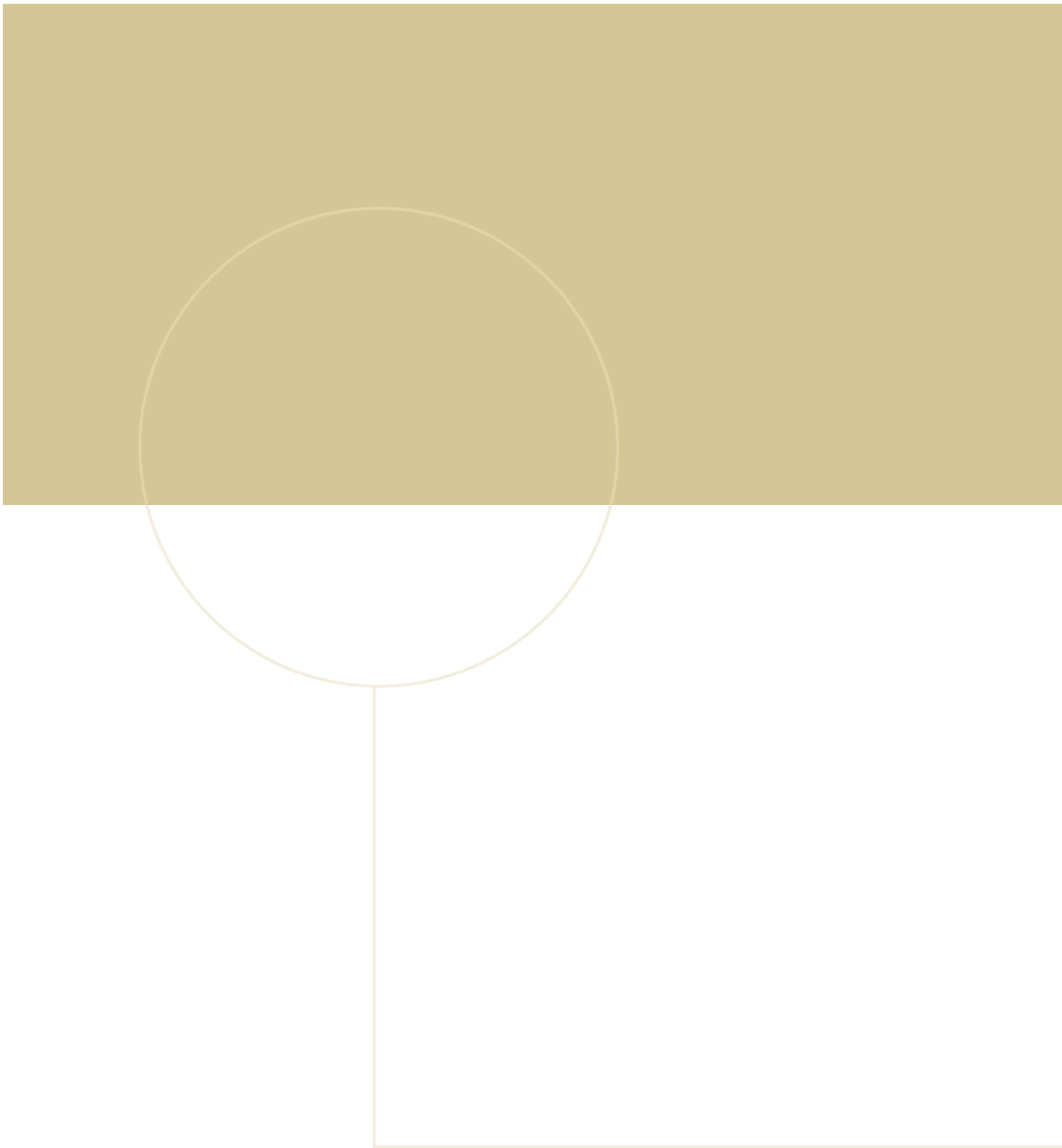

NTNU
Norwegian University of
Science and Technology